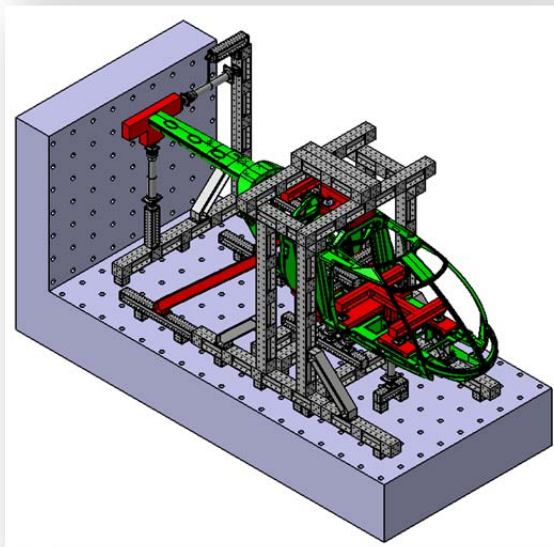


REVIEW
OF AERONAUTICAL FATIGUE INVESTIGATIONS IN SWITZERLAND
APRIL 2013 – MARCH 2015



DR. MICHEL GUILLAUME | ZURICH UNIVERSITY OF APPLIED SCIENCES
SCHOOL OF ENGINEERING | ZAV CENTRE FOR AVIATION

REVIEW
OF AERONAUTICAL FATIGUE INVESTIGATIONS IN SWITZERLAND
APRIL 2013 – MARCH 2015

ZAV DOCUMENT 2015

Dr. Michel Guillaume
Zurich University of Applied Sciences
ZHAW / School of Engineering
Centre for Aviation

SUMMARY

The Swiss review summarizes fatigue work in Switzerland. It includes main contributions from the Zurich University of Applied Sciences (ZHAW), RUAG Switzerland Ltd. (RUAG Aviation). This document forms a chapter of the ICAF conference minutes published by the conference host nation. The format of the review reflects ICAF requirements.

Prepared for the presentation at the 34th ICAF Conference

Helsinki, 1st and 2nd June 2015

SUMMARY	1
4.1 Introduction	3
4.2 Automatic Stress Intensity Factor Calculation based on the Elastic Energy Release Rate Method Coupled with the NASTRAN FEM Solver	4
4.3 Automated Calculation of Stress Concentrations around Holes	9
4.4 F/A-18 Vertical Tail Stub FEM	12
4.5 Evaluation of the Structural Impact of Pitting Corrosion Damage on a Lower Wing Skin	16
4.6 Clean Sky / Eco Design ITD, Testing of A4 Demonstrator	19
4.7 Development of a test concept for the Swiss Marenco SKYe SH09 Helicopter	23
4.8 Crack propagation in adhesive transverse to load direction	25
4.9 Assessment for Repairs of Engine Structural Components	27
4.10 Structure Analysis of Aging Airplane Engine Mount	29
4.11 References	34

4.1 Introduction

The present review gives a brief summary of the work performed in Switzerland in the field of aeronautical fatigue, during the period from May 2011 till March 2013. The various contributions to this review come from the following sources:

- Zurich University of Applied Sciences (ZHAW); School of Engineering, Institute of Material Processing & Centre for Aviation
- RUAG Switzerland Ltd., RUAG Aviation; Structural Engineering
- SR Technics Switzerland Ltd.
- Marengo Swisshelicopter Ltd.

All the interesting contributions are gratefully acknowledged, especially the effort of Gregor Peikert (ZHAW) and Andreas Uebersax (RUAG Aviation).

4.2 Automatic Stress Intensity Factor Calculation based on the Elastic Energy Release Rate Method Coupled with the NASTRAN FEM Solver

Thierry Stehlin, Raphael Rigoli, Ingrid Kongshavn, Raphael Zehnder, Christoph Kunz, Mark Weber / RUAG Aviation, Michel Godinat / armasuisse

In order to perform crack growth (CG) analysis, the knowledge of the stress intensity factor (K) or of the stress intensity correction factor (β) at the crack tip is mandatory. Commercially available software packages such as AFGROW and NASGRO provide β solutions for standard cases. However, for complex geometry and loading conditions, standard solutions are not appropriate anymore and an alternative method is required. A tool using the energy release rate concept was developed (pyNASSIF), which permits the calculation of K for up to 2 thru crack fronts in virtually any thin structure. It is based on a NASTRAN FEM model using PLATE elements with pre-defined crack paths. The cracks are implemented in the FEM model by unzipping the nodes along the crack path. The process of running the model at several cracks sizes and extracting the necessary information (cracks lengths, crack increments, material properties, plate thickness and elastic-energy) to perform the calculations is automatized in pyNASSIF, whose main output is β as a function of the crack length. In the case of two crack fronts, the output is a set of two β matrices, one for each crack tip, with dependence on tip 1 and tip 2 lengths. β solutions can then be exported to CG analysis software to perform the CG calculations. Using this method, complex structural behavior with geometrical non-linearities and/or contacts can easily be assessed, and in the case of multiple load path analysis, the load redistribution between the primary member and the secondary member is automatically accounted for. Validation of pyNASSIF was done by performing comparison of β solutions with other commercially available programs such as AFGROW, NASGRO and FRANC2D for several standard cases (SE-TM-14-001, pyNASSIF Theory and Manual, Jan 2014).

This analysis approach was used to perform the study on one of the cracks found during the tear down inspection at the end of the FSFT of the Swiss F/A-18 performed by RUAG. The inspection revealed a 16in long crack in the outer wing spar 3 in the spanwise direction along the web to bottom flange interface (about 1/4 of the spar was severed, see **Figure 1**).

The crack growth was not obvious to explain and no standard model was applicable to such a case. The use of pyNASSIF combined with the R-Curve method and AFGROW runs resulted in:

1. A better understanding of the crack path and the final crack lengths found in the test article. Note that all CG modes [I, II and III] were active at different stages of the CG.
2. An explanation of the quasi-static failure followed by subsequent crack growth observed by quantitative fractography (QF).
3. The development of a total life model for fleet support.

The background for the FEM model is the Swiss F/A-18 global FEM (GFEM), from which a sub-model (SFEM) of a portion of the inner and outer wing was derived. For the crack initiation (CI) and the thru-the-thickness CG analyses, a SOLID mesh of spar 3 was

implemented in the SFEM. For pyNASSIF and subsequent CG analyses, a detailed model (DFEM) of the spar 3 using PLATE elements was implemented in the SFEM, see Figure 2. A typical limit load case was chosen as reference load case to perform the analyses.

The failed component was analysed using QF, to identify the site of crack initiation. The crack initiation location coincided with a 3D stress concentration in the model, at the lower flange to web transition corresponding to a flange thickness change. The FEM analysis using the SOLID mesh showed that the position of the highest calculated maximum principal stress was consistent with the test findings. The calculated crack initiation life at this position was 3'200 spectrum flight hours (SFH).

Thru-the-thickness crack growth analysis was performed assuming a 0.01" semi-elliptical crack at the crack initiation position and using the stress gradient obtained by the FEM with SOLID mesh. The calculated crack growth life for this phase is 2'550 SFH.

In order to perform the internal thru crack analysis, the crack path had to be defined. Depending on the crack propagation mode, the criteria for crack path definition is different. For mode I, the crack tends to grow in a plane perpendicular to the maximum principal stress. For modes II and III, the crack tends to grow in the direction of the maximum shear stress. Therefore, in the case of the F/A-18 outer wing spar 3 crack, two possible paths were analyzed on both tips and the one leading to the highest β was selected for each tip as presented in Figure 3.

After the K solution was developed using pyNASSIF, the R-curve method was used to assess the critical crack length. On tip 1 (Figure 4), the crack was stable until it reached the first outer wing rib. At this position, the stress intensity was drastically reduced and the crack growth was almost stopped. The analysis at crack tip 1 is in agreement with the FSFT end crack position. At crack tip 2 (Figure 5), the R-curve analysis showed that the crack was instable along a portion of the end of the spar when the crack started to grow vertically along the vertical flange. Then the crack growth was stable again until it stopped when the tip reached the top flange. At this stage, the crack was mostly loaded in compression. The analysis results are in agreement with the QF findings, which showed an instable crack growth pattern along a portion of the vertical flange at the end of the spar, followed by stable crack growth. The calculated final crack length on tip 2 is also in agreement with the crack found at the end of the FSFT.

The total life model was then defined as the sum of the CI and CG lives as shown in Figure 6.

In the FSFT article, a strain gage was positioned just above the path of tip 1. During the FSFT, the SG showed a signal drop between 8'000 and 9'000 SFH, which means that the crack passed below the SG during this period, see Figure 6. According to the analysis, the crack would be expected to pass below the strain gage at about 8'000 SFH. Therefore, it was concluded that a very good agreement between calculated crack growth speed and the strain gage signals was found.

The model developed using pyNASSIF was validated with the findings of CI location, crack path, final crack length and portion with instable CG as well as the CG speed. Therefore, it can be used with a flight spectrum to perform an efficient and reliable fleet survey.

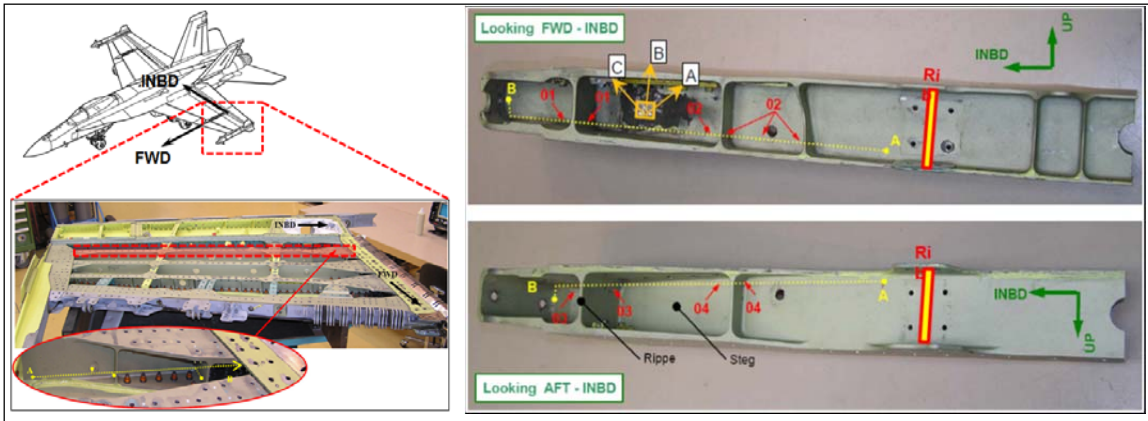


Figure 1: Crack in Outer Wing Spar 3

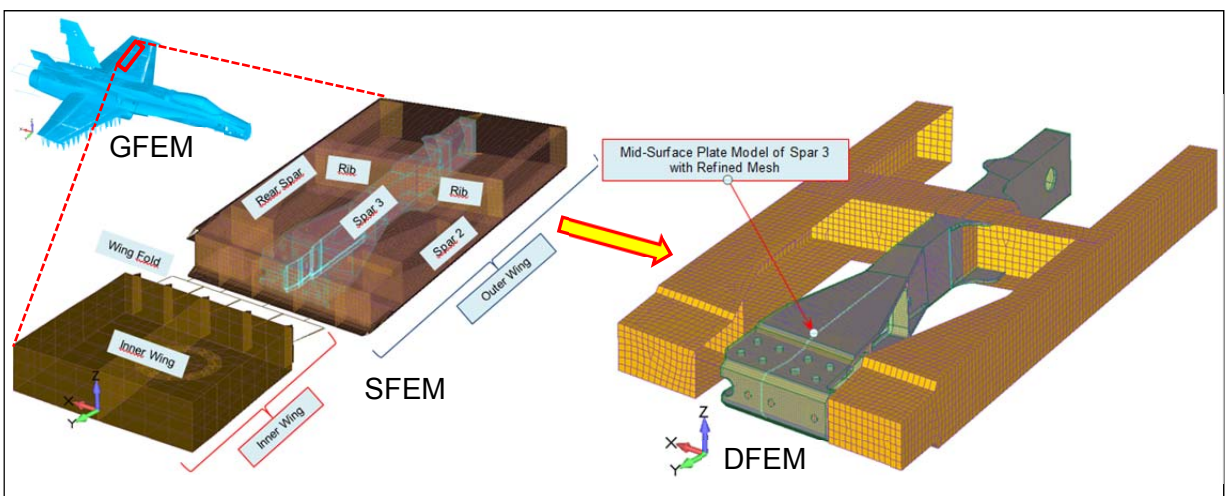


Figure 2: Finite Element Models

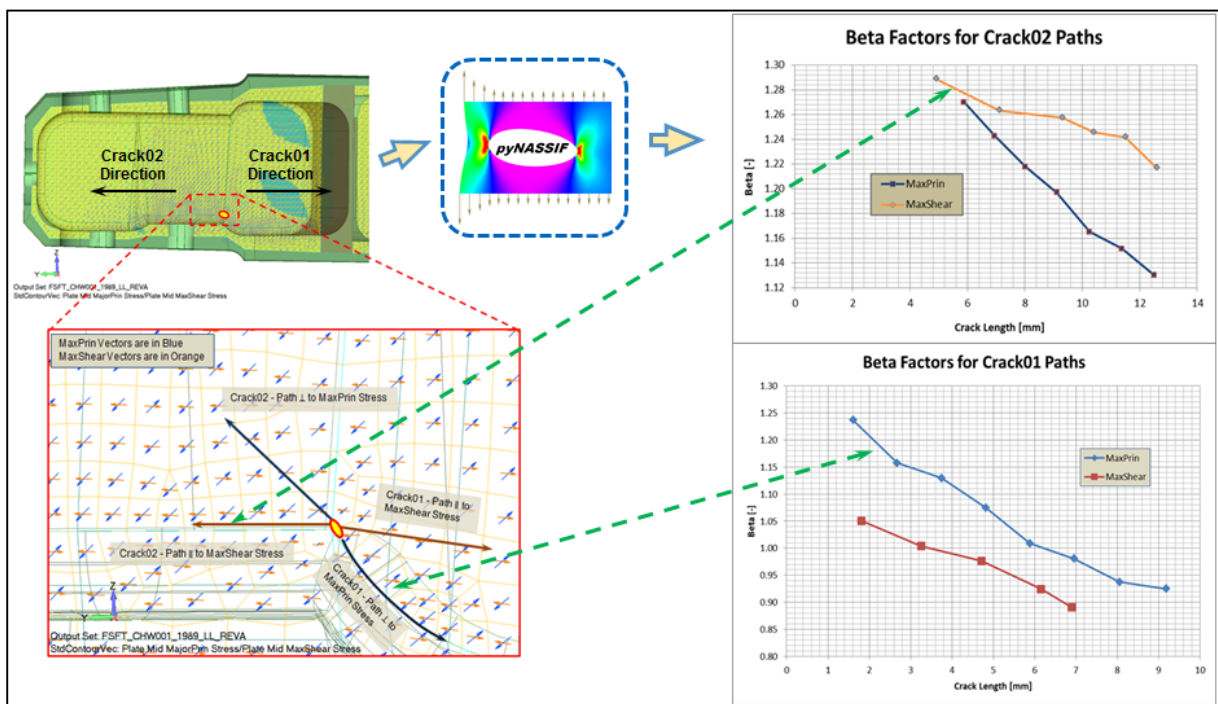


Figure 3: Crack Path Assessment

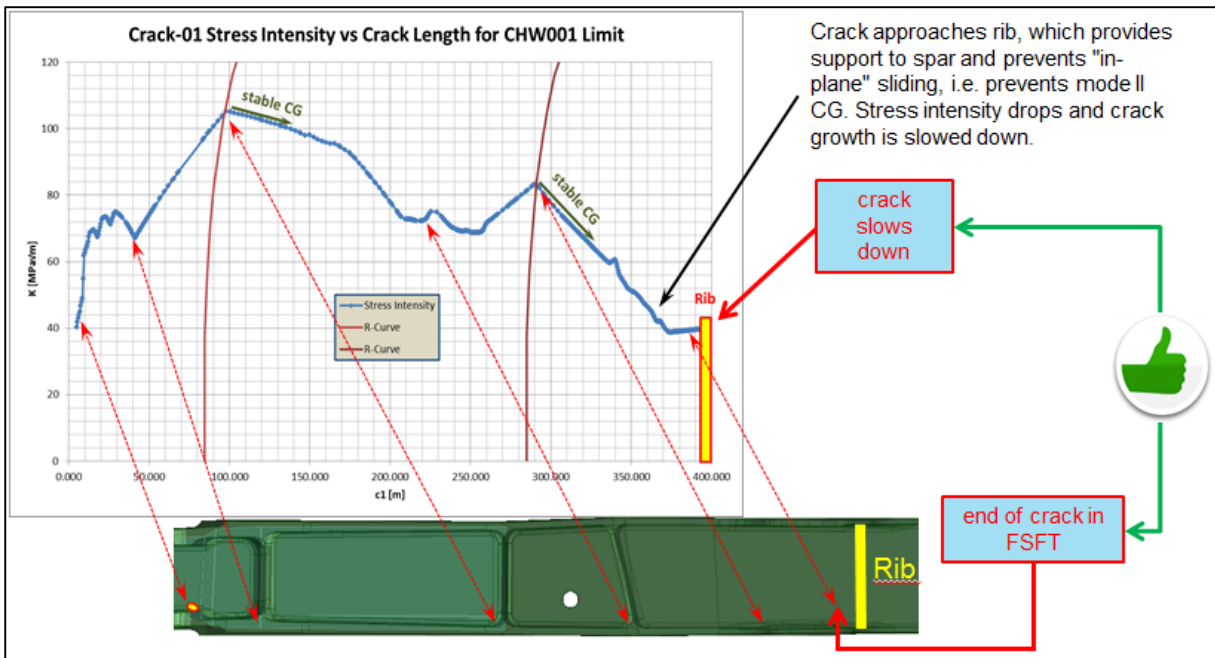


Figure 4: Stress Intensity Solution and Critical Crack Length for Tip 1

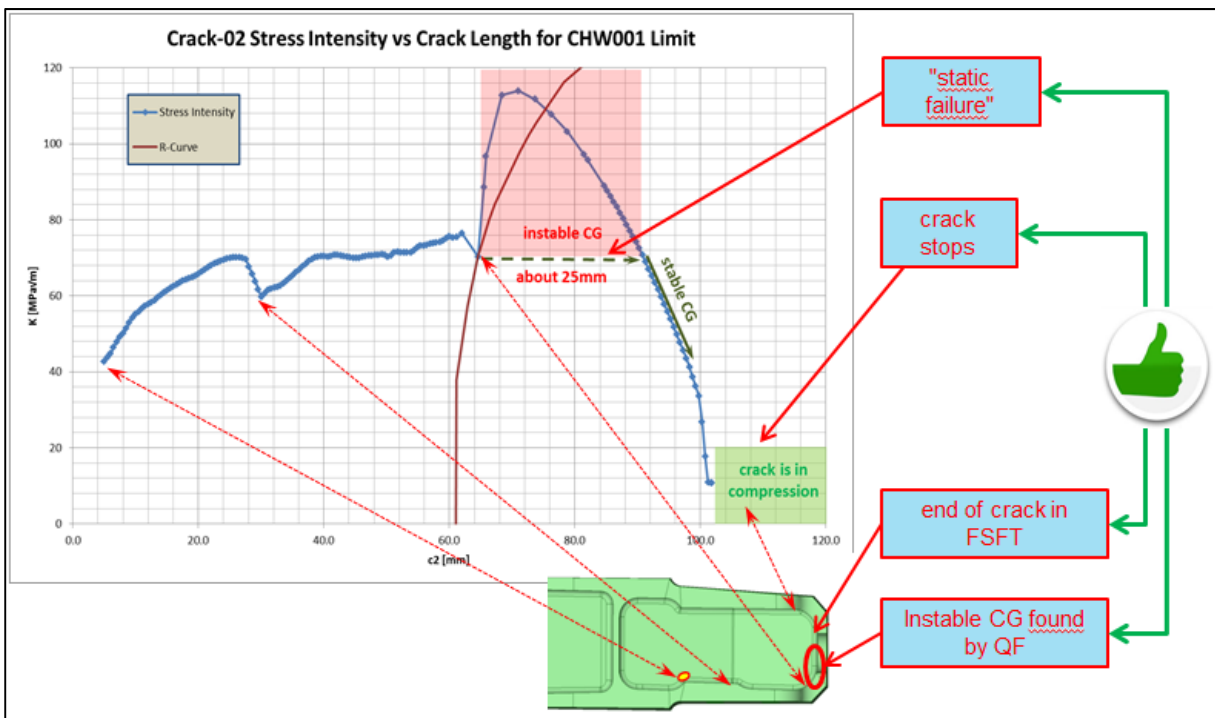


Figure 5: Stress Intensity Solution and Critical Crack Length for Tip 2

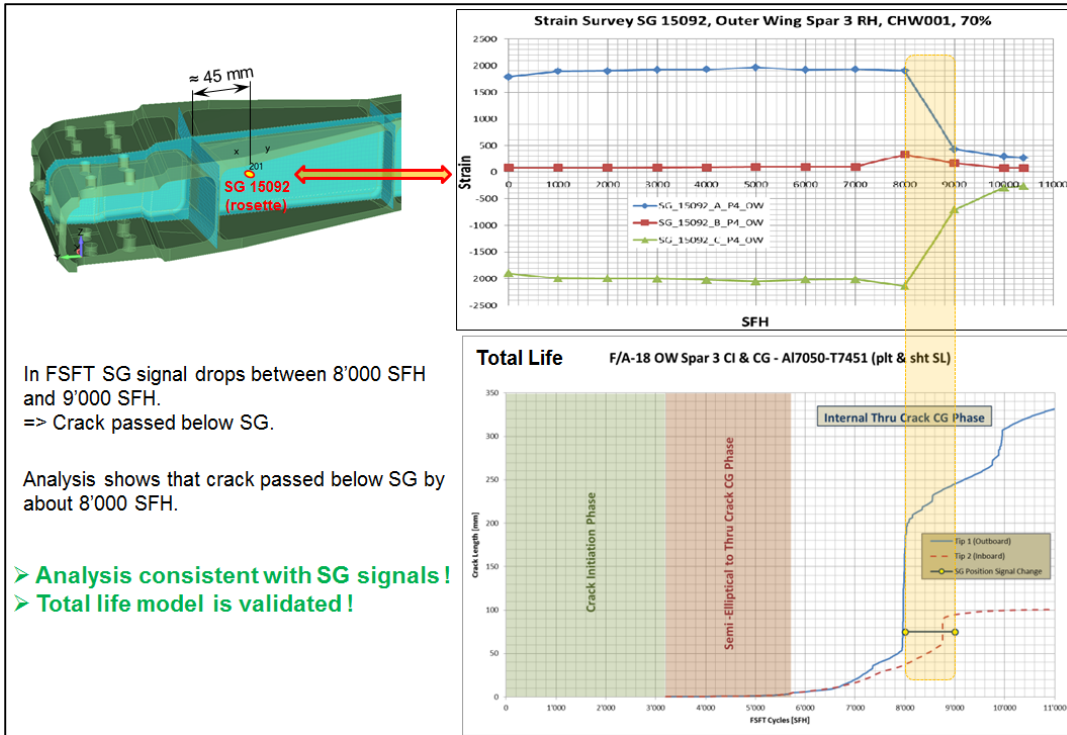


Figure 6: Total Life (CI + CG)

4.3 Automated Calculation of Stress Concentrations around Holes

Luzian Michel, David Schmid, Christoph Kunz, Thierry Stehlin, Mark Weber / RUAG Aviation, Michel Godinat / armasuisse

Precise modeling of stress concentrations is critical for the fatigue life assessment of structural parts. An important and frequent source of such concentrations are fastener holes. Fatigue analysis of the stresses around the holes typically consists of a multi-step process. Loads at the edges of a small rectangular surface patch around the hole are first extracted from a detailed FEM. Afterwards, the loads are divided into several basic load cases (e.g. unloaded hole with thru stress only) for which stress concentration factors are available from the literature. Finally, a clocking analysis has to be performed. Some of these steps have to be performed manually which causes the process to be time consuming and error prone.

To circumvent this lengthy and error-prone process, RUAG Aviation has developed a modern automated tool for the analysis of fastener hole stresses. The basic idea behind this tool is to use FE-based results instead of pre-calculated literature values. The working principle of the tool is shown in Figure 7. In a first step, the user defines the areas containing fastener holes to be analyzed (represented as 2D FE-element sets, see Figure 8) and selects the subcase from which the loads have to be extracted. The tool automatically recognizes fasteners, creates a freebody of the surface and extracts all necessary information such as element geometry, sheet material and thickness, loads and fastener details. Afterwards the tool

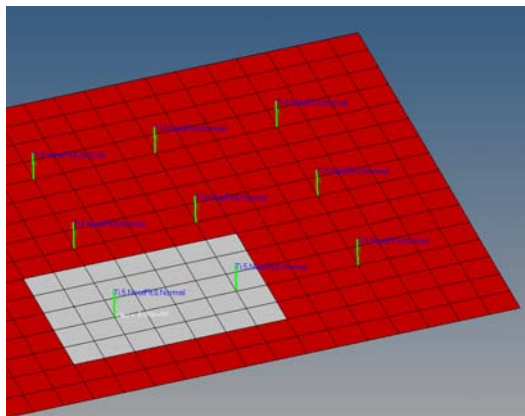
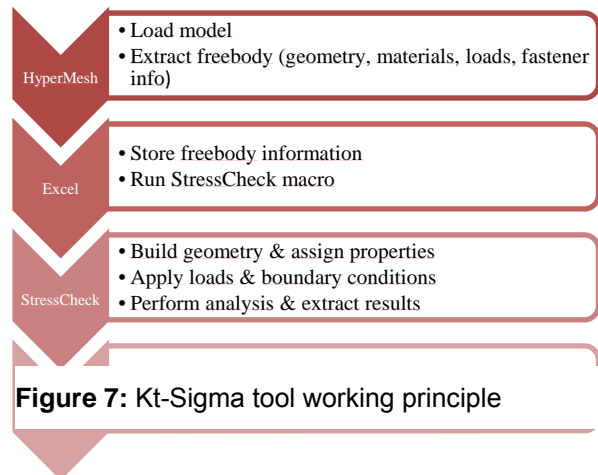


Figure 8: Example surface patch in DFEM

creates a 3D-FE model of the extracted 2D freebody. For the generation and analysis of the 3D model, a special p-type FE-Software called StressCheck is used. The advantage of this software is that quick and accurate results can be achieved due to the fact that the result quality is relatively independent of the mesh density around the fastener hole and thus the mesh can be kept coarse. The geometry of the 3D model is based on the 2D elements from the DFEM as Figure 9 shows. Once the 2D geometry has been recreated, the sheet is extruded through the thickness and the fastener holes are subtracted. After meshing (using the software's Automesh capabilities), the loads are applied. Loads on the sheet boundaries are applied at mid-thickness on element faces closest to the original position of the extracted point load. Fastener loads are distributed on the hole interfaces according to Figure 10.

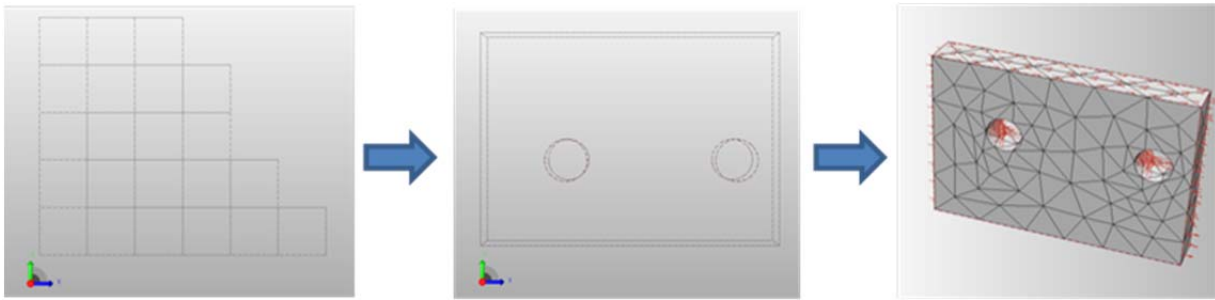


Figure 9: 3D model creation steps in StressCheck.

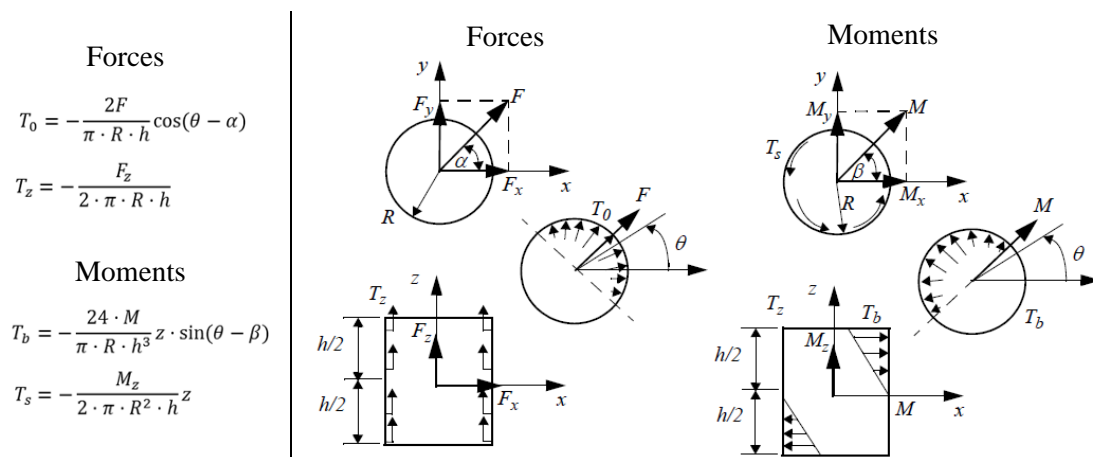


Figure 10: Fastener load distribution. (StressCheck 9.2 Master Guide, p. 261, ESRD, 2011)

After the calculation of the model, the max principal stress around the model is evaluated. This is done at three locations: top, bottom and mid-thickness. The results for each fastener present in the surface patch are written to a results sheet.

The tool was evaluated by calculating several model cases and checking the results against literature values. For example, FE results for a lug which is loaded at a varying angle were compared to standard curves from the literature. The Kt values at low angle match quite well, whereas significant differences at higher load angles are found. Generally peak values of the FEM are higher compared to the literature values. Interestingly, at a load angle of 180° according to the literature, Kt values are the same everywhere around the hole, which is not confirmed by the StressCheck FEM. The evaluation of the same lug model with a different mesh on a different solver confirmed the results obtained from the StressCheck model.

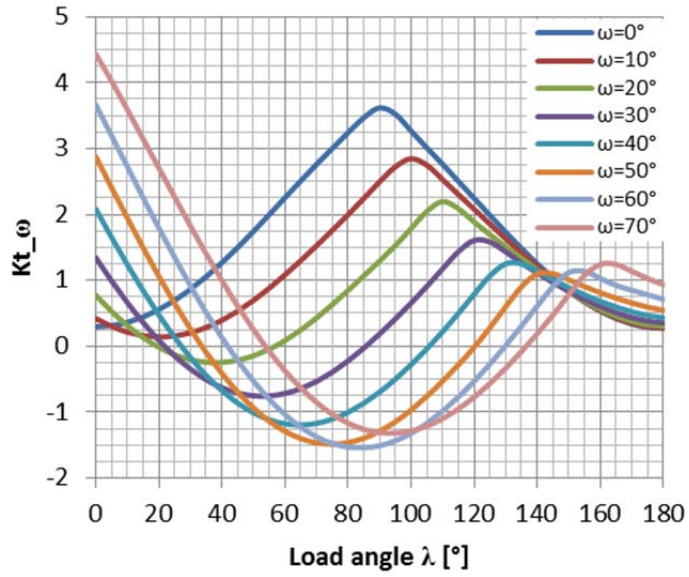


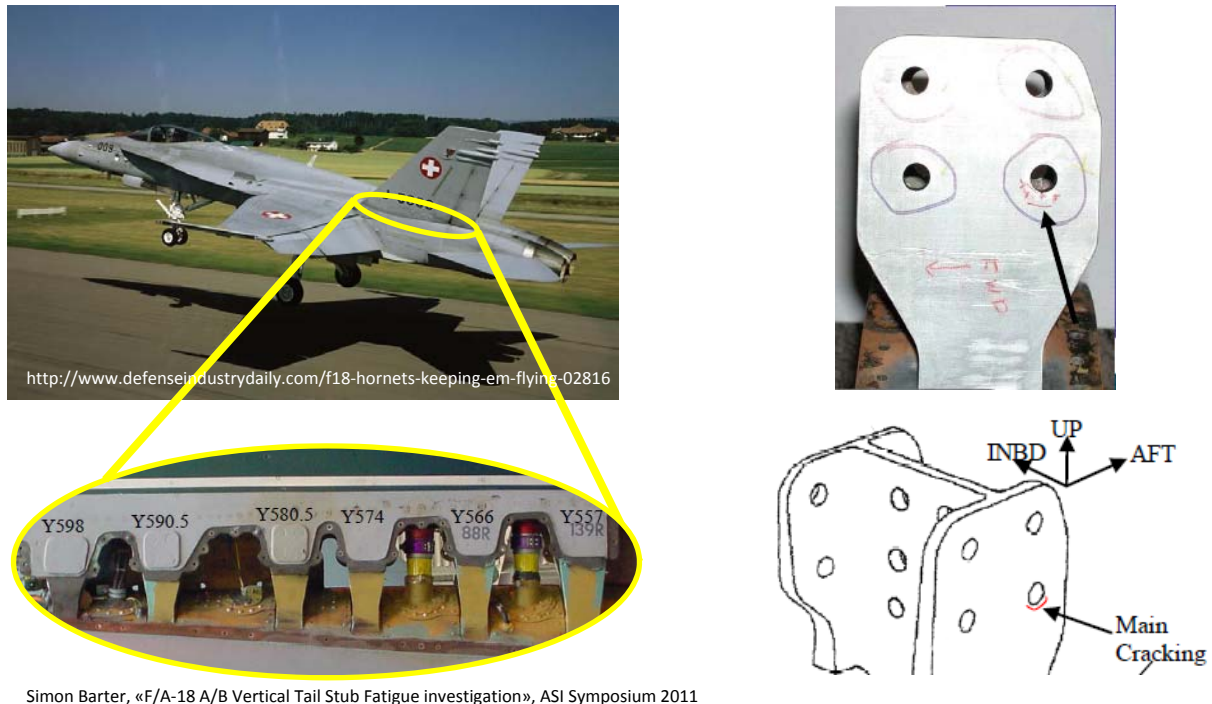
Figure 11: Max principal stress plot, lug case (λ as load angle and ω as location around hole with 0° being the orientation of a standard lug).

In the future, the tool will be expanded to include additional stress concentrations, such as those caused by countersinks as well as pin bending.

4.4 F/A-18 Vertical Tail Stub FEM

Luzian Michel, David Schmid, Ramon Nebel, Christoph Kunz, Thierry Stehlin, Mark Weber / RUAG Aviation, Michel Godinat / armasuisse

The F/A-18 Vertical Tail is attached to the fuselage via 6 stubs (Figure 12). During inspections, cracks were found near the fastener hole interfaces by several operators. Ref. [1] The location and direction of the cracks indicate that they are not caused by bearing loads. Several studies have already been conducted on this topic to identify the root cause for the cracks.



Simon Barter, «F/A-18 A/B Vertical Tail Stub Fatigue investigation», ASI Symposium 2011

Figure 12: FA/18 vertical tail location & crack location. Ref. [1]

Based on the idea that friction load transfer plays an important role, RUAG Aviation investigated this topic in detail. A detailed solid FE contact model of the stub-to-skin joint was created (Figure 13). The model was subjected to a simple symmetric tension load and different contact conditions (stick, slip and friction) were compared to each other.

In a first step, max principal stress distributions on the stub surfaces were investigated. Figure 14 shows that for the slide contact configuration, high stresses are found directly at the hole interfaces as expected, whereas for the stick contact configuration high concentrations are found at crack locations. Apparently the reported cracks could indeed be caused by sticking behavior of the contact.

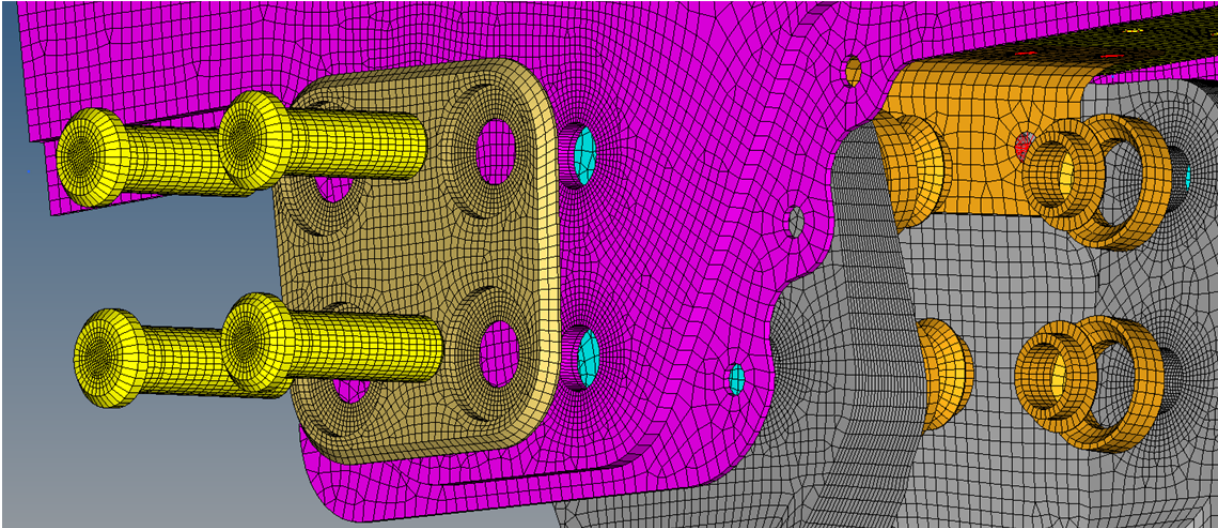


Figure 13: Vertical tail stub FE model.

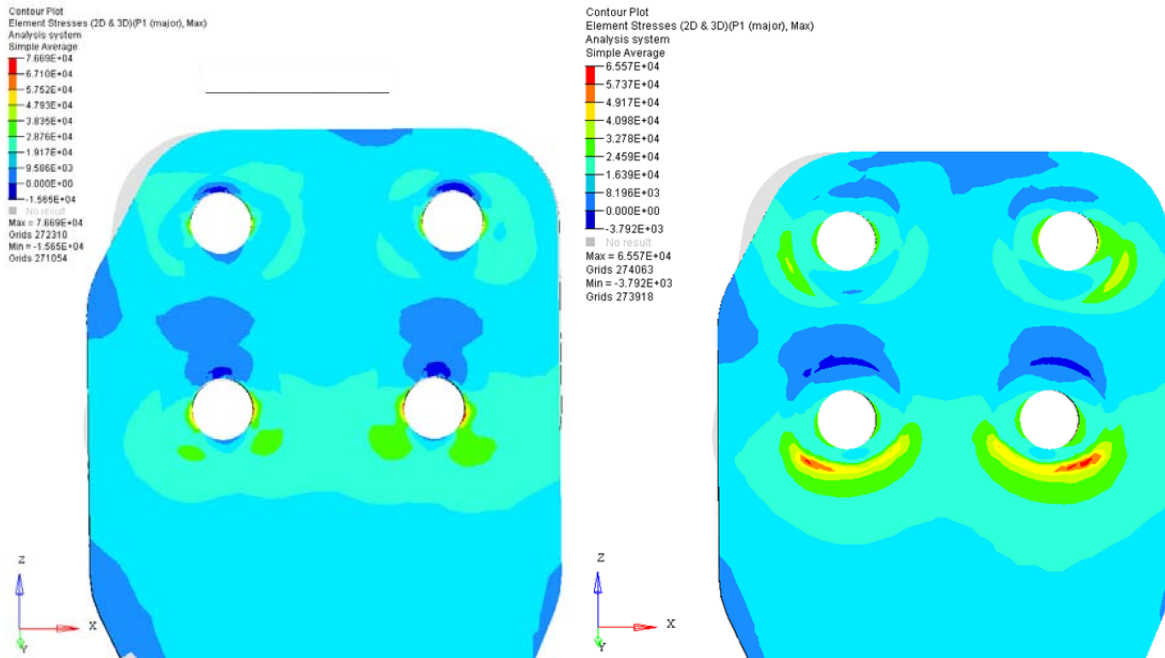


Figure 14: Max principal stress contour plots, slide configuration (left) and stick configuration (right).

For the friction contact configuration, plots were created with different amounts of load. One can see that until 60%-80% of the final load, some stress concentrations at crack locations are visible. At 100% of the applied load however, bearing stress concentrations at hole interfaces dominate, indicating that slippage occurs between 80% and 100% of the applied load.

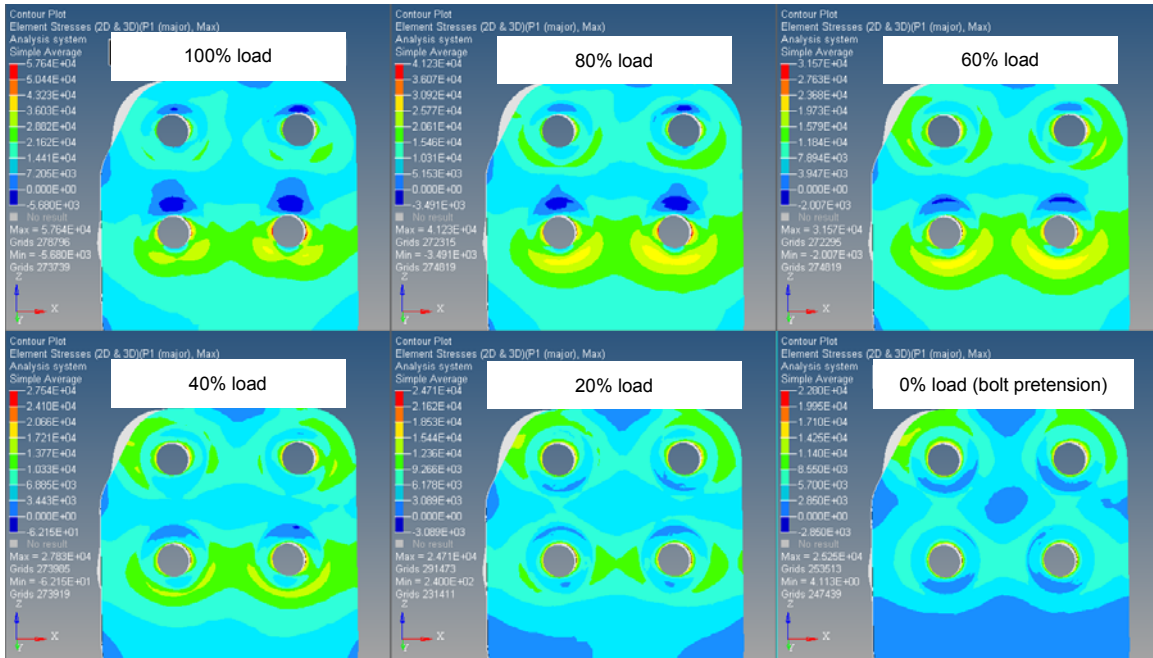


Figure 15: Max principal stress contour plots, friction configuration for different load magnitudes.

To check the plausibility of these assumptions, the hole elongation was investigated. The idea behind this was that deformation of the holes should only occur if the surfaces would slip against each other.

Figure 16 shows an example plot of the lower left hole. The differences in stick/slip behavior of the three configurations is clearly visible. There is almost no deformation for the stick configuration as expected. Interestingly there is almost no elongation for the slide configuration until up to 40% of applied test load. This may be explained by residual stresses in the hole being present due to the interference fit fasteners which have to be compensated before elongation starts. Finally the point of slippage for the friction configuration can be identified. It appears that the surfaces tend to stick until the load exceeds 60% of the applied load. At higher load slippage starts.

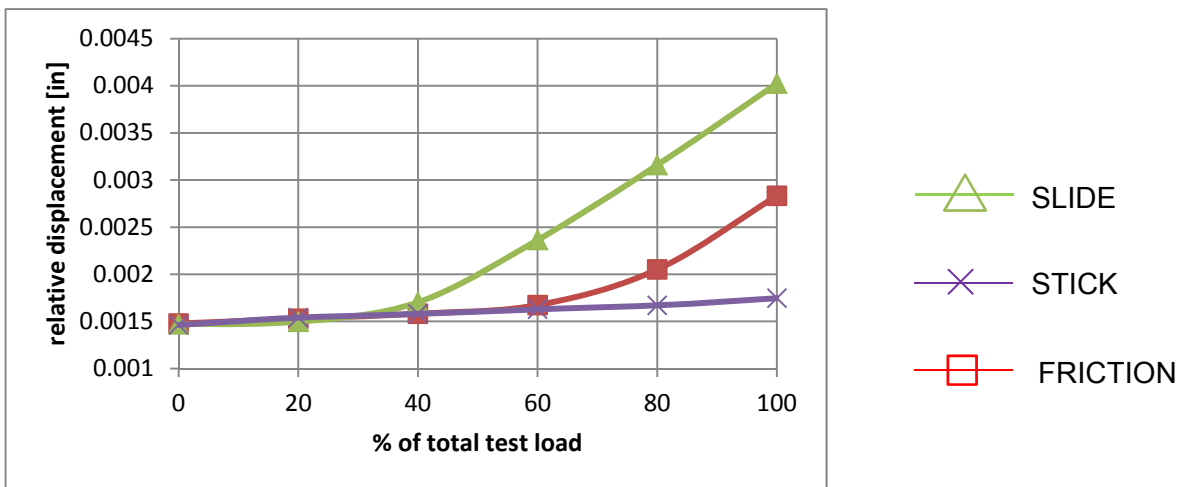


Figure 16: Hole elongation measurements for different load magnitudes.

The study shows that while the friction model offers a possible explanation for the reported cracks, other factors may need to be included in the model. For example, more realistic loads (derived from flight maneuvers) involving asymmetric bending and/or

torsion rather than symmetric tension should be applied. A more accurate calculation of the bolt pre-tension force should be performed and the friction coefficients should be reviewed. Furthermore, a component test could be performed in order to calibrate the FE model.

4.5 Evaluation of the Structural Impact of Pitting Corrosion Damage on a Lower Wing Skin

A. Uebersax, R. Zehnder / RUAG Aviation, G. Renaud, M. Liao / National Research Council, Canada

Several projects in the context of assessing and managing corrosion damage in fighter aircraft wing skins have been performed by RUAG Aviation in the last few years.

As the presence of corrosion is usually not taken into account by the original equipment manufacturer in the design phase, it has to be removed when detected in service. This “find it and fix it” philosophy leads to cost penalties and availability shortfalls. Attempts are often made to move away from this approach and to manage corrosion damage so that it can be rectified within scheduled maintenance.

The present work tries to address these issues by showing an engineering application for evaluating the structural impact of pitting corrosion damage in a fighter aircraft aluminium lower wing skin. Aluminium 7075-T7351 flat dog-bone test specimens with an open straight-shank hole were used to substantiate the proposed approach. Pristine as well as artificially corroded specimens were fatigue tested to failure. The corroded specimens were produced with pitting corrosion in three different magnitudes. The pitting was produced in the centre section of the straight-shank hole, as this location presents the most critical and conservative area for additional damage. Fatigue tests were run with a Mini-Falstaff wing bending spectrum with added constant amplitude marker bands for post-test quantitative fractographic investigations.

It was observed in the tested coupons that cracks nucleated within the pits, but not necessarily at their deepest points. Typically, multiple crack nucleation origins were found at each pit, see

Figure 17. Crack growth curves were recorded by quantitative fractography for each test specimen. Two different methods were then used to back-calculate equivalent initial damage sizes that can be used to characterize the pre-existing corrosion damage in a damage tolerance assessment: first the traditional back-calculated Equivalent Initial Flaw Size (EIFS) with a crack growth model that is based on fracture mechanics, and second the Equivalent Initial Pre-Crack Size (EPS) according to the Lead Crack Fatigue Lifting Framework methodology of [2], which assumes a log-linear crack growth behaviour. Both approaches showed good correlation in equivalent initial damage sizes. It was noted that the equivalent initial damage sizes correlated reasonably well with the average pit sizes. Therefore, once the existing corrosion pit sizes are known, the remaining fatigue lives can be calculated.

The initial engineering framework that was developed in this work will help the engineer to assess the impact of corrosion damage and to develop appropriate repair actions. It consists of the following steps:

1. Determine the average pit dimensions. If not enough pit data is available, determine the largest pit depth.
2. Assume that the pit depth determined in Step 1 equals the average EIFS or EPS.
3. Calculate the crack growth life of a critical location with the EIFS or EPS for pitting corrosion.
4. Divide the calculated crack growth life by an appropriate safety factor.

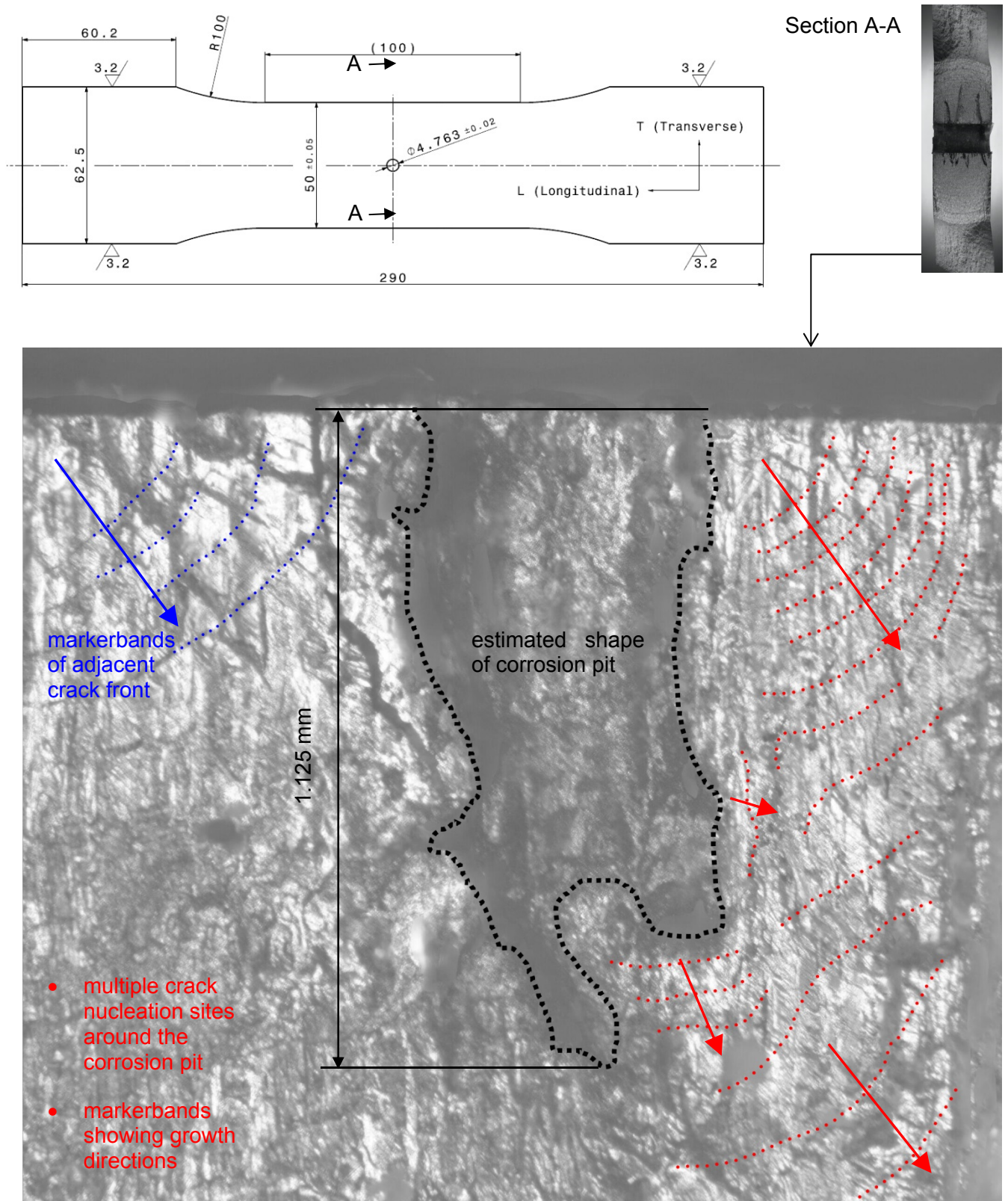


Figure 17: Severe corrosion pit with visible marker bands within centre section of straight hole test specimen

Once the pit dimensions are known, such a framework will provide the structural engineer with a simple method to assess the impact of corrosion on the structural integrity of a lower wing skin. This framework is the engineering basis to decide whether to repair or to allow corrosion to remain in service for a limited period of time, i.e. delay

the repair until a convenient scheduled maintenance and therefore potentially lower costs and increase fleet availability.

The application of two different approaches to calculate an initial pitting corrosion damage (EIFS or EPS) is shown. It is left open to the respective organization to determine which approach should be applied in the specific case.

A similar project was finished in 2010 for intergranular corrosion damages on a wing upper skin (aluminium 7075-T651 and compression dominated loading spectrum), see Ref. [3].

This project is performed in collaboration with the Aerospace Portfolio of the National Research Council Canada (NRC).

4.6 Clean Sky / Eco Design ITD, Testing of A4 Demonstrator

B. Bucher, B. Schmid / RUAG Aviation, U. Stebler, M. Danzi / ETHZ

Introduction

The Clean Sky JTI (Joint Technology Initiative) [4] is one of the largest European research projects ever, carried out over the period from 2008–2016 with the following environmental goals:

- 50% reduction of CO₂ emissions through drastic reduction of fuel consumption.
- 80% reduction of NO_x (nitrogen oxide) emissions.
- 50% reduction of external noise.
- A green product life cycle: design, manufacturing, maintenance and disposal/recycling.

The project is divided into 6 technology domains / ITD's (Integrated Technology Demonstrator) including Eco Design. The Technology Evaluator gathers data from each ITD and evaluates the new green conceptual aircraft based on the results of the ITD's. The Eco Design ITD focuses on green design, production and optimal use of materials, thus reducing the environmental impact.

Switzerland is participating in this project as a RUAG Cluster (RAC). RUAG is the cluster leader and the participants are RUAG, ETHZ, EPFL, FHNW, Huntsman, CYTEC and HADEG.



Figure 18: Clean Sky with 6 ITD's

Technology Demonstration

In order to validate the performance of the new technologies developed in the Eco Design ITD, a total of 12 demonstrators are being built and tested. The RUAG cluster (RAC) is responsible for the A4 demonstrator, which addresses the low energy curing technologies of carbon reinforced composite. This includes inductive curing using the Huntsman developed paste adhesive system LEM10625/10626, the application of MTM44-1 out of autoclave prepreps from CYTEC and phenoxy bonding using weldstrips, a technology developed by NLR.

The A4 demonstrator is based on a DO228 aileron architecture and aims to validate a total of 7 implemented new technologies at the technology readiness level (TRL) 6 [5].

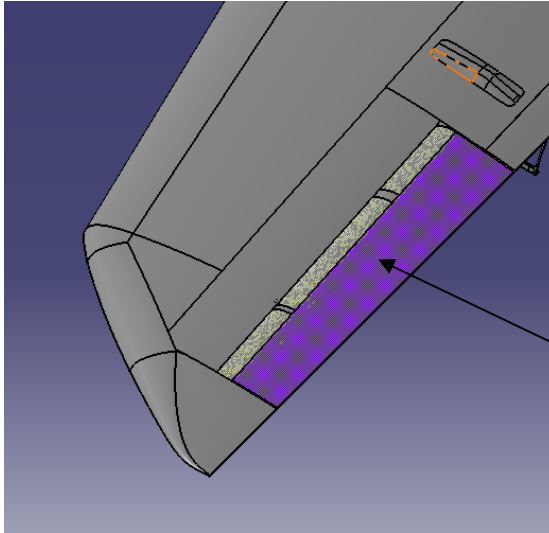


Figure 19: Outer Loft Surface Model on CATIA 5 for DO228 L/H Wing and Aileron

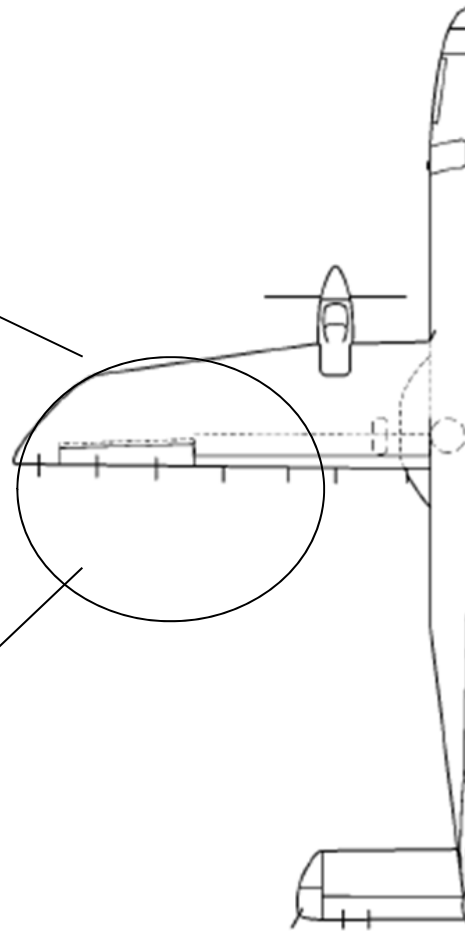


Figure 20: Plan View of L/H side of A/C

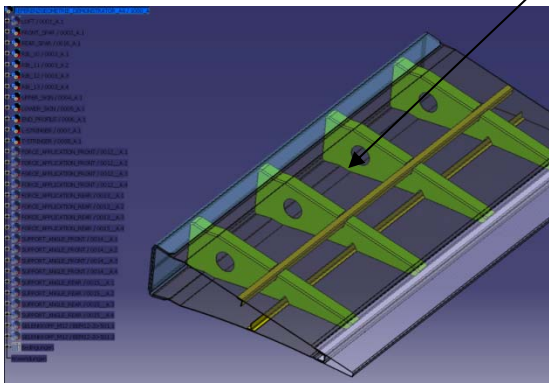


Figure 21: Simplified Baseline DMU Model in CATIA 5 of A4 Demonstrator

Mechanical Testing

For the validation, three demonstrators were built. Two demonstrators were mechanically tested in a 4 point bending configuration. The performance of the demonstrator A4-1, which incorporates new technologies, was compared to the demonstrator A4-ref, which incorporates current technologies.

In June 2014, RUAG Aviation in Emmen successfully completed the mechanical testing that consisted of strain surveys, fatigue cycling and rupture. Fatigue cycling was run in a dry laboratory environment (20 °C) at approximately 2 Hz test frequency and at a load level equivalent to an 80% limit load case that included a load enhancement factor of 20%. This additional enhancement factor was required to account for environmental effects (hot/ wet and cold) that were not simulated during the tests. Only tensile loads were applied using a MTS servo-hydraulic test bench with an R-ratio of 0.1. Fatigue cycling was completed for both demonstrators without damage propagation of artificial flaws (AF) and barely visible impact damages (BVID's). Buckling of the upper skin panel was observed close to each peak load.

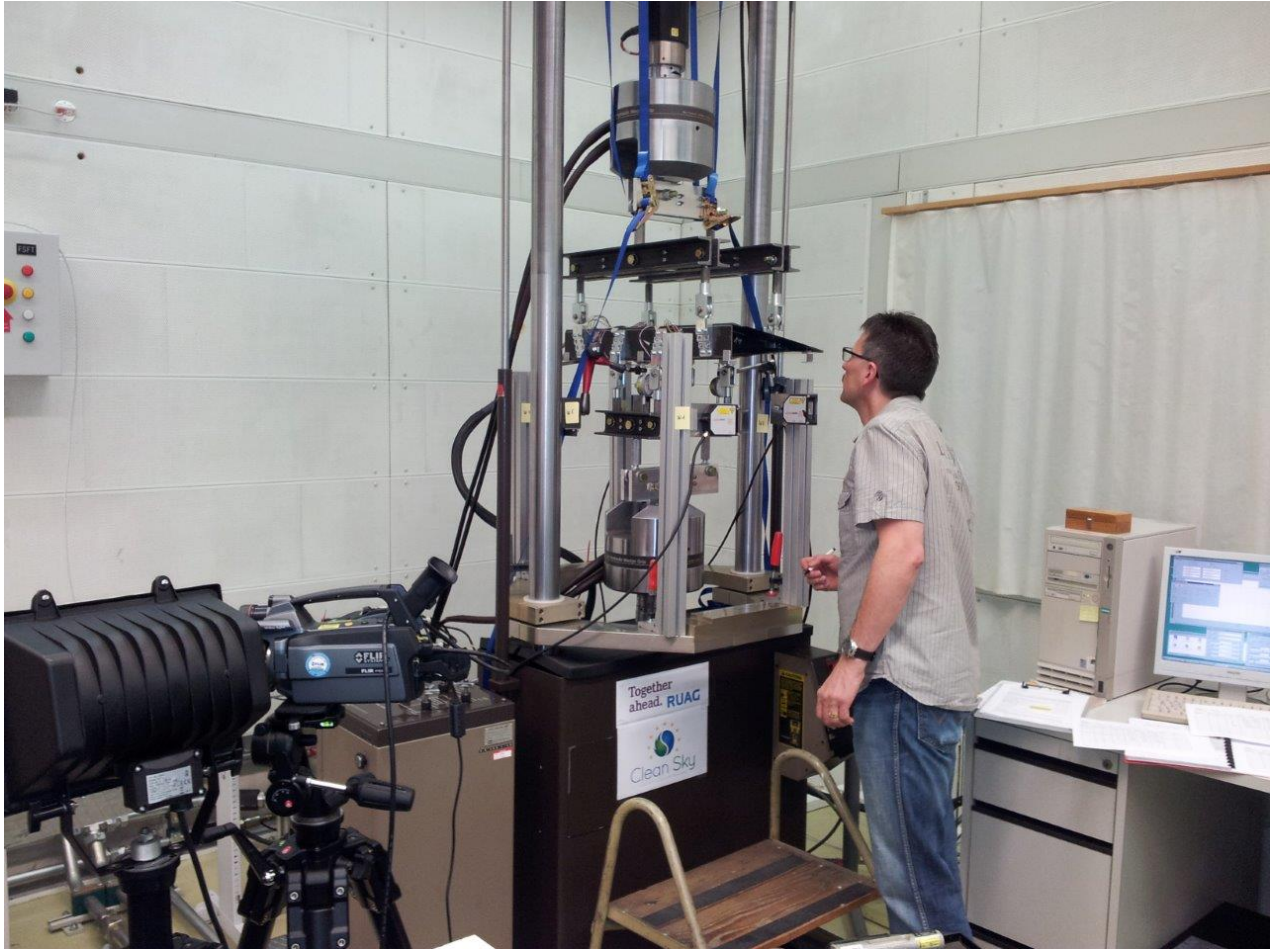


Figure 22: Test Set Up for Static, Fatigue and Rupture Testing

Analysis of Test Results and Conclusions

The test data (displacements, strains, buckling) has been checked for consistency and was subject to more detailed analysis. It was shown that in general a good correlation between test and analytical FE strains, displacements and buckling pattern was achieved. Work to correlate the rupture loads observed in the test with the analytical models (FEM) is still progressing.

Patran 2008r2 Pre-Release 13-Oct-14 14:08:35

Deform: 4ptb_AFTCP, PW Linear : 100. % of Load, Displacements, Translational.

A4 Demonstrator

4 Point Bending

Displacement Magnification 10

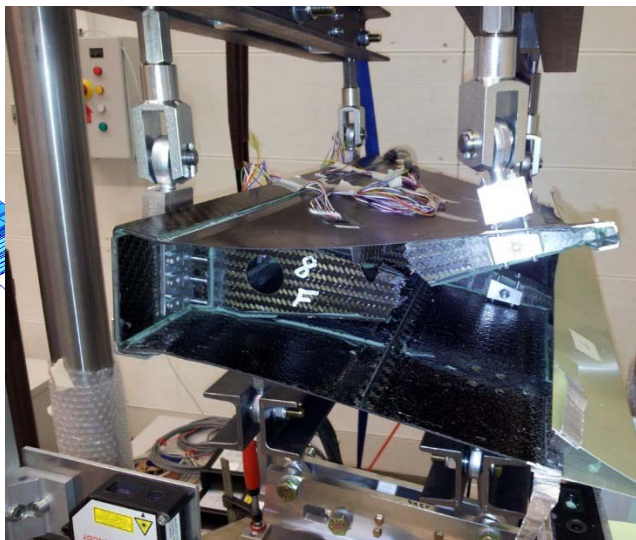
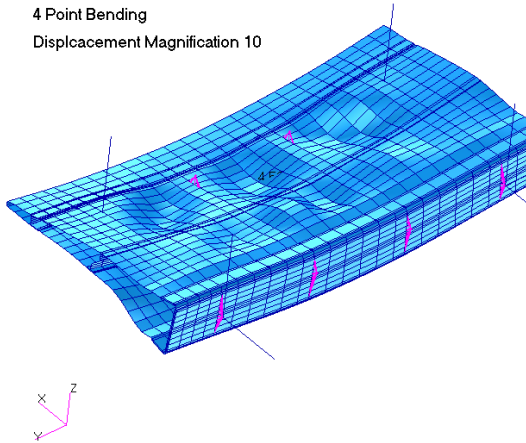


Figure 23: Non Linear Analysis using **Figure 24:** Rupture of A4-1

Nastran SOL106

It is also currently being investigated, which failure mechanisms can be attributed to the final rupture and to what extent AF's (Artificial Flaws) and BVID's (Barely Visible Impact Damages) have contributed to the rupture mechanism.

An extensive tear down was performed [6] and cross- sections were cut to assess the quality of skin-stringer connections. Two examples are shown in the next pictures.

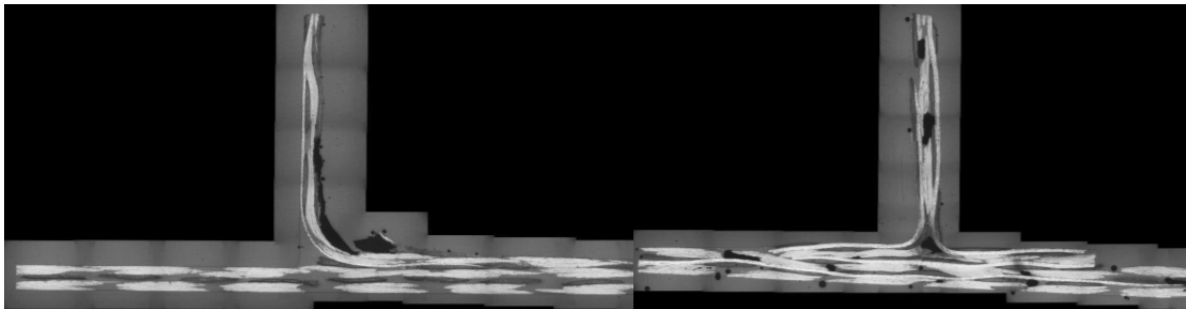


Figure 25: L-Stringer – Skin Connection of Upper Skin

Figure 26: T-Stringer – Skin Connection of Lower Skin

In general, the parts produced with the CYTEC MTM44-1 out-of-autoclave prepreg and the LRI L-stringer showed good quality. For the bondlines, excessive porosity was observed in all cases: for the inductive cured Huntsman LME10625/10626, the oven cured LME10625/10626 and the oven cured reference paste adhesive Henkel Hysol 9394. It is assumed that the porosity is attributed to the paste adhesive mixing process that resulted in excessive air bubbles in the adhesive.

Further work will be necessary to achieve the target cured paste adhesive porosity of 2% typically required for bonding processes without vacuum.

4.7 Development of a test concept for the Swiss Marengo SKYe SH09 Helicopter

Michel Guillaume[°], Rudolf Fuchs[°], Matthias Frei[°], Felix Steinmann[°], Daniel Schuhmacher[°], Simon Wyss[°], Manuel Flepp⁺, Silvain Michel^{}*

[°] Zurich University of Applied Sciences / ZHAW

⁺ Marengo Swisshelicopters AG

^{} Empa – Swiss Federal Laboratories for Materials Science and Technology*

The Zurich University of Applied Sciences was tasked to develop a detailed concept for the conduction of static load testing (preliminary development test) to achieve successful certification of the structure for the helicopter SKYe SH09 (see Figure 27) of the company Marengo. The new helicopter SKYe SH09 is a light single engine helicopter fully built by a composite structure. The helicopter can be used for several services, such as transport, rescue, surveillance, etc.

The main challenge of the project lies in the fact that experience of the aviation industry concerning the conduction of such testing is not shared in public. Therefore, the achievement of conducting successful load tests for certification of the helicopter in Switzerland is a big task when never done before. To master the posed challenges, Marengo decided to team up with the research organization Empa (Swiss Federal Laboratories for Materials Science and Technology) which is experienced and in possession of the necessary infrastructure (actuators, load cells, measurement and control systems).

In a first step, the design load cases based on EASA CS27 were analyzed and 4 basic load conditions were selected to develop the test concept. The test rig should also be used for a future fatigue test. The goal is to build a test system with methods that are as simple as possible to achieve successful, efficient test performance. To do so, different practices have been used to reach an appropriate outcome.

During the first activities, a basic test concept was proposed based on access to the helicopter structure and the structural test floor at Empa (Figure 28). Some hard points at the structure were defined in collaboration with Marengo. 5 push-pull actuators will be used for the test. The sling load case will be tested at the end of the test as well. The test article will mainly be constraint at the rotor head because it offers a lot of potential to react all the test loads. For the design of the test rig, a lot of standard steel parts from Empa can be used. To simulate the loads on the cabin, pilots, passengers, cargo, and inertia forces from heavy parts will be simulated and introduced via a specially whiffle trees. During 4 months, a complex system at the rotor head was constructed using load cells to monitor the loads and moments.

At the moment, the detailed design for the whole test set up is ongoing. Based on actual planning, the test should start in spring 2016.



Figure 27: First prototype of SKYe SH09

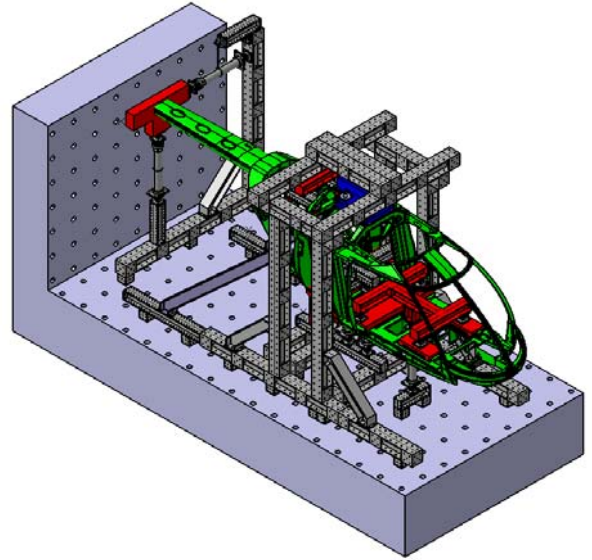


Figure 28: Preliminary concept for the static test

4.8 Crack propagation in adhesive transverse to load direction

Gregor Peikert

Zurich University of Applied Sciences / ZHAW

The Institute of Material Process and Engineering is part of the EU frame work7 project BOPACS, together with the aerospace companies Bombardier, Airbus and EADS. One of the major tasks is to implement crack stoppers (Figure 30) in adhesive bonded composite materials. Test samples were developed for mode II and III crack propagation. The impact of crack stoppers was evaluated using special surface treatments with NDI methods. The test confirmed that crack growth transverse to the load direction can be achieved.

Dynamics tests with strain amplitude of 300 microstrains tensile load were done at R ratio of 0.1. The carbon epoxy specimen consists of 3 mm bonded with epoxy paste adhesive.

A final application test will be made on the aileron flap of the Bombardier CRJ700 airplane.

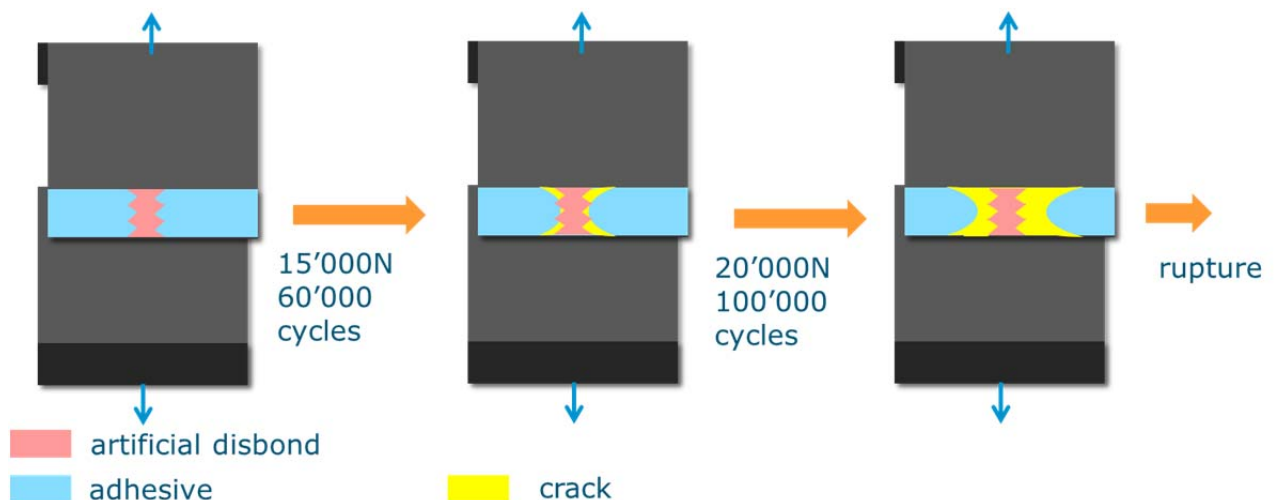
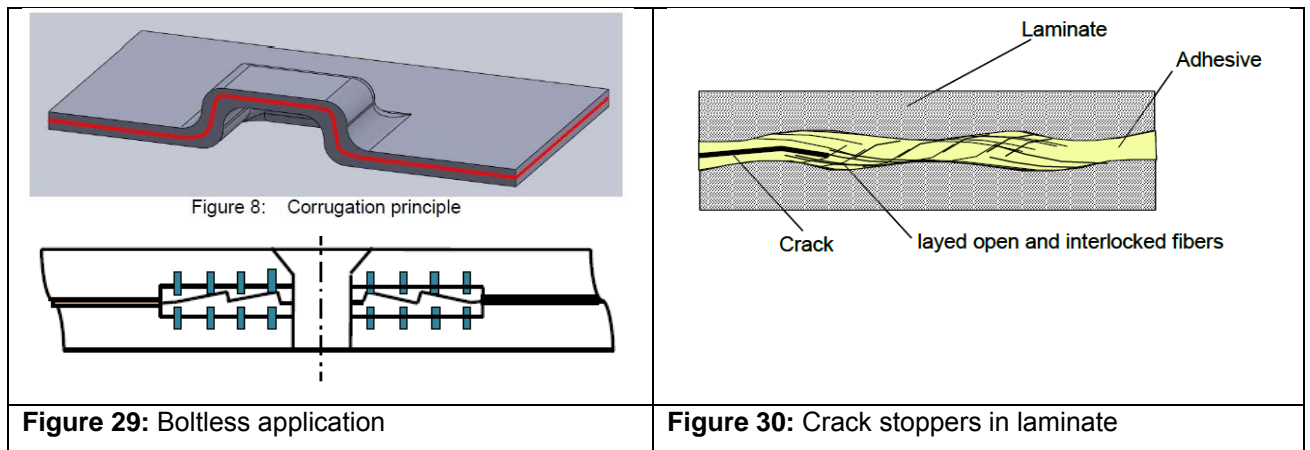


Figure 31: Dynamic test procedure of carbon epoxy specimens



Figure 32: Application of developed technology on aileron of Bombardier CRJ700

4.9 Assessment for Repairs of Engine Structural Components

Michel Guillaume⁺, Tobias Fuchs⁺, Nicolas Pfenninger⁺, Joel Kempter⁺, Elias Pertschy⁺, Tomas Valenta^{}*

⁺ *Zurich University of Applied Sciences / ZHAW*

^{*} *SRTechnics, Zurich*

Jet engines are very complex systems with a lot of structural parts. Some of them are not only affected by cyclic loading of mechanical stresses but also due to thermal stresses.

SR Technics is in the business of maintenance and overhaul of large commercial jet engines.

If the structural parts are out of tolerances or structural damages are detected during overhaul the parts will be scrapped. The costs for new parts mount up to several hundred thousand USD. Hence, SR Technics tasked the Zurich University of Applied Sciences to do an assessment for repair capabilities of the exhaust nozzle PW4000-100 (Airbus 330) and the fan frame shroud of the CFM56-7B (Figure 33, Boeing 737 NG). The CFM56-7B has some changes compared to the CFM56-5B used on the Airbus 320. The fan frame for CFM56-7B shroud consists of three parts; the outer frame is made of 2219-T6 and the strut hub is Ti-6Al-4V. For the CFM56-5B the whole is one part made of steel 17-4PH.

For the exhaust outer cowl, a new repair method with rivets instead of welding was proposed. To check the new solution and better predict the friction forces of rivets, tensile tests were undertaken by SR Technics using Ti-6Al-4V sheet with riveted fasteners (several types of fasteners with different heads). Based on a Berkeley-Madonna model, the temperature gradient was calculated to determine the impact of thermal stresses for the proposed new repair.

Several inspections on multiple CFM56-7B engines showed corrosion spots on the surface (Figure 34) and in the holes on the fan frame shroud. Several factors were considered in order to figure out which kind of corrosion is damaging the structural part. Important was the analysis of the different materials involved in the assembly. The result confirmed the complex situation of fretting, pitting, and contact corrosion. The first conclusion of the OEM was that pitting corrosion is the only source of damage. Several grinding out processes depending on the depth of damage were analysed. For the holes, bushing repair solutions were studied and discussed.

In the meantime CFM adopted the results of the studies and issued a bushing repair for the particular holes.

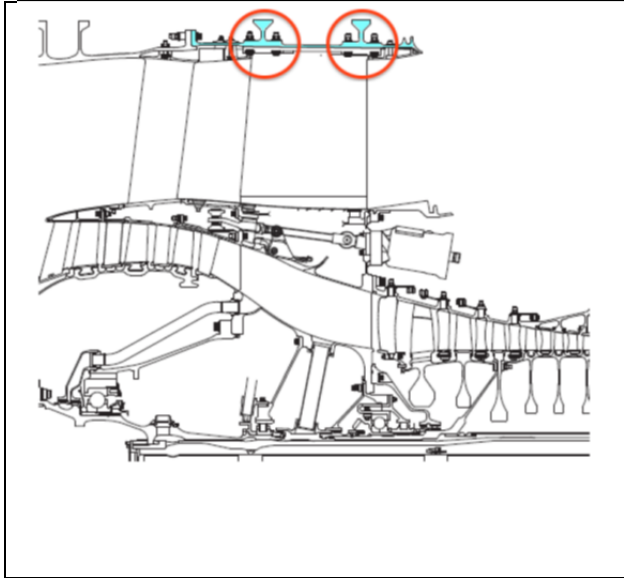


Figure 33: Fan frame shroud CFM56-7B (blue)

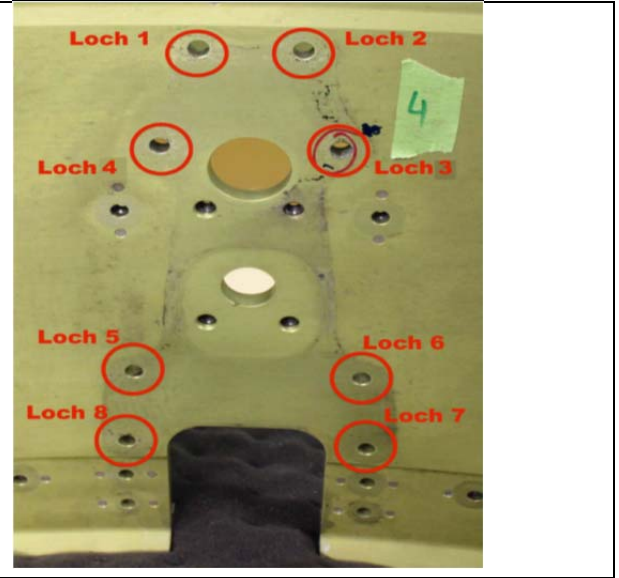


Figure 34: Holes with corrosion damages

4.10 Structure Analysis of Aging Airplane Engine Mount

Michel Guillaume, Elias Schläpfer, Marcel Schmid

Zurich University of Applied Sciences / ZHAW

Introduction

Today the fleet leaders of the Pilatus P-3 trainer under civil operation are close to the tested life of 5'000 FH. The civil usage of these old planes may be quite different compared to the military usage. Nevertheless, the safe operation is a demand and has to be approved by experienced fatigue engineers. A further challenge is the documentation of past experience. In this report, the procedure for the Pilatus P-3 will be discussed and a detailed structural analysis of the engine mount will be presented.

The P-3 full scale fatigue test performed in 1960 showed minor damages which were all addressed in modifications for the whole fleet. During the military service life, no cracks were discovered during inspections (intervals of 100 FH, 200 FH or once a year) and no special incidences for structural damages were reported.

In 1975, a structural integrity study was done to assess the fatigue life of the fleet. The Swiss fleet was cleared to 3'000 FH and 12'000 flights due to the less severe usage compared to the full scale fatigue test.

The Swiss Air Force retired the P-3 fleet in 1995. The P-3 were sold as "oldtimers" to private people. In Switzerland 17 aircraft received a civil registration by FOCA. The military service schedule was converted for civil usage. The P-3 had between 3'000 and 3'400 FH during military usage.

The current fleet leader has accumulated 4'270 FH whereas another plane has done less FH but reached already 4'872 landings. The P-3 full scale fatigue test demonstrated no failure at 5'000 FH and 10'000 landings. This means that the P-3 showed a safe life of 2'500 FH and 10'000 landings. According to the structural integrity study of 1975, the fleet leader exceeded the cleared limit of 3'000 FH. Therefore, further investigations are needed to ensure the continuing safe operation of the civil registered P-3 airplanes.

Assessment for Civil Usage

First, the available Nz spectrum from the military usage were analyzed and compared to the full scale fatigue test spectrum. Second, two Swiss operators were interviewed to understand the civil usage. We can conclude as a result that the P-3 are no longer flying spins and do not exceed 5G's. Most flights are within 1 to 2G; during special displays, the P-3 flyers of Airolo still fly loopings with higher G but 5G seems to be the real limit. This information is very limited for making engineering analysis concerning the remaining life of civil usage. The civil usage may be heavily depending on the operators.

Nevertheless, an assessment was done with collecting all the data from the military usage and reviewing the information.

The risk matrix of International Civil Aviation Organization (ICAO) was used to rank the status of the P-3 structure regarding safe operation. In general, the structure of the P-3 has hazardous risk severity with improbable risk probability, see Figure 35 graphic (dark box).

Risk probability	Risk severity				
	Catastrophic A	Hazardous B	Major C	Minor D	Negligible E
Frequent 5					
Occasional 4					
Remote 3					
Improbable 2					
Extremely Improbable 1					

Figure 35: Result of ICAO risk matrix for P-3, and critical areas of P-3 structure

The critical areas were found to be:

- engine mount fairing; not tested
- landing gears; not tested
- vertical tail, not tested
- connection between inner and outer wing; high loads transfer, bolts were already replaced in service

No service failures or cracks were reported and documented. After the changes due to residual static test in the fleet, no

modifications were done.

In a review with the FOCA, it was decided to do a static analysis and fatigue investigation on the engine mount (priority 1). These fairings were never tested but are safety critical. A crack could lead to fatal failure which must be avoided in any circumstance.

4 Structural Analysis of Engine Mount

For loads selection the EASA standard CS23 was applied:

- Steady state maneuvers CS23.361
- Gust load CS23.361
- Side load maneuver CS23363
- Horizontal spin maneuver CS23.361
- Side load on ground CS23.485
- Ground load condition as reference for fatigue analysis (weight on wheels condition)

For engine conditions, CS23.423 and AMC23.371 was also used. To get all the loads, the flight manual was necessary, together with the data from the Lycoming engine model GO-435-C2 and the propeller information from Hartzell; their help is gratefully acknowledged.

The engine mount is a tube structure with welded connection with steel material 4130 [1], see Figure 36 below; general simplified layout and detailed picture (aft connection to engine = Motorlasche).

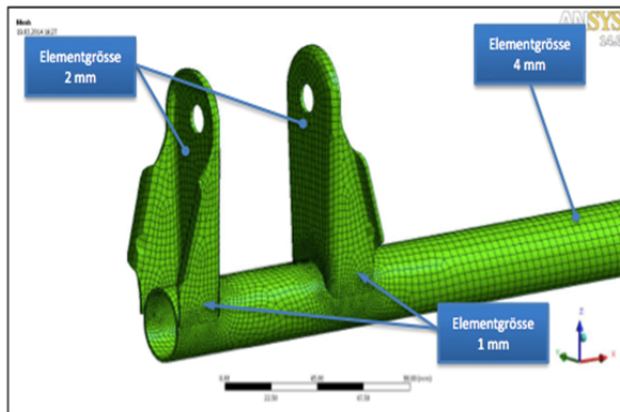
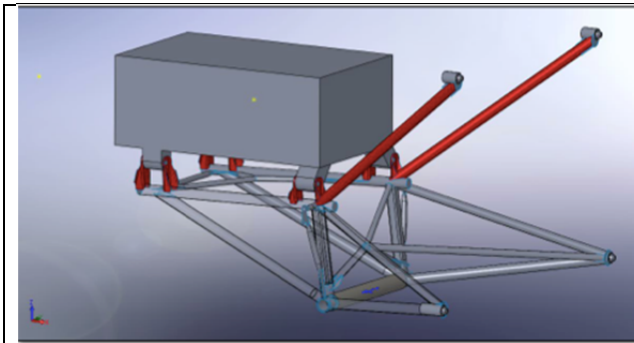


Figure 36: Engine mount structure with FE model



Figure 37: Detailed picture of aft engine mount fairing

All the required loads could be calculated without any problems.

The FE code from ANSYS was used to develop a finite element model. First, a simple model was designed, followed by a more complex model. The engine itself was simplified as quadratic bloc. For details, see the FE model in Figure 36 with element sizes of 1, 2, 4 mm depending on structural required details. To determine the correct size for surface FE model, a grid converge study was done which results in a mesh size of 2 mm and 4 mm for a tube diameter of 15 mm.

In this FE model, the welds were not modeled. For the connection of the tubes ANSYS Workbench "bonded" approach was used. In the connection area the mesh size was further reduced to 1 mm.

To improve the model especially at the connections and interfaces the FE model was locally refined using a submodel with volume mesh elements. The welds were simulated with a typical radius.

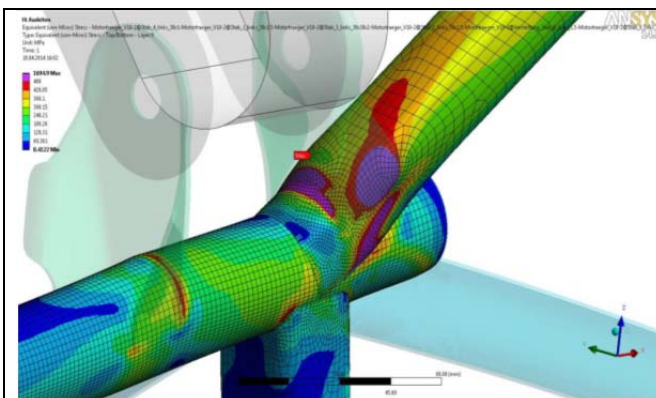


Figure 38: Critical stresses based on FE analysis,

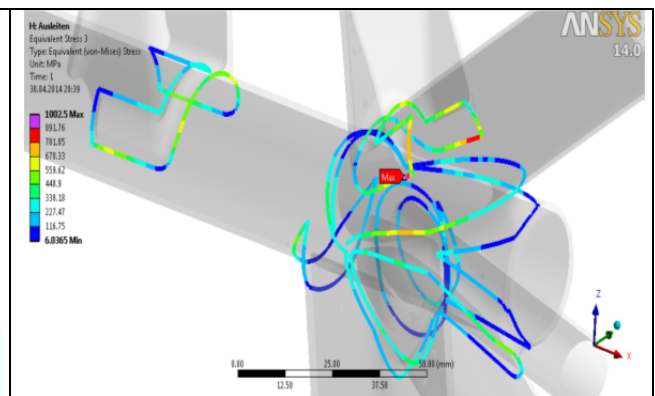


Figure 39: CAB detailed analysis for structure.

The results of the FE model showed large deformations of 4 to 4.8 mm at left hand forward engine mount fairing. The static analysis was based on the FKM requirements. Based on the static strength analysis the ultimate load cases of steady state 6G maneuver and horizontal spin maneuver exceeded the tensile strength of steel 4130. Local plasticity was not modeled in detail which would give more accurate results.

Fatigue Investigations

Based on the spectrum information from the test and the Nz exceedance data for the Swiss Air Force usage, a Rainflow Counting Matrix was developed. A lot of knowledge of the period of Mirage III test development has to be applied to determine the 32 by 32 Rainflow Counting Matrix.

With the corresponding FE results for the Nz values, the spectrum could be converted to stresses at the critical locations based on principal stresses of the sub model FE data. For the critical locations (engine connection aft = *Motorlasche* and upper bolt connection to forward fuselage frame = *Anschlussbolzen*) the stresses in function of Nz.

For fatigue investigations the flying steady maneuver loads are contributing to the fatigue damage. In the first approach MIL-HDK-5J data, see Figure 38, for steel 4130 at stress concentrations $kt = 1.5$ and of $kt = 2.0$ was used for max min stress level to see if the fatigue life is in the area of durability life. This kt values are considered because the *Motorlasche* has the kt of 1.25 and the *Anschlussbolzen* a kt of 2.0. The max stress for the *Motorlasche* was 35.5 ksi respectively 45 ksi for *Anschlussbolzen* at mean stress of 20 ksi. Both values are below the red dotted curve at 10^7 cycles, see Figure 40. This confirms that the two locations have a durability life.

To get more confidence in our analysis, we also used the local strain life approach with strain life curves. Therefore, the strains from the detailed FE models at the two critical locations (*Motorlasche* and *Anschlussbolzen*) were taken into account. Using strain life data with stress ratio of $R = -1$ we observed strain amplitudes of 0.14% (*Motorlasche*) respectively 0.23% (*Anschlussbolzen*). The strain amplitude of 0.23% showed 100'000 cycles up to failure whereas 0.14% showed infinite life. The stress ratio of the real cycle is about 0.4 which yields a higher number of cycles up to failure.

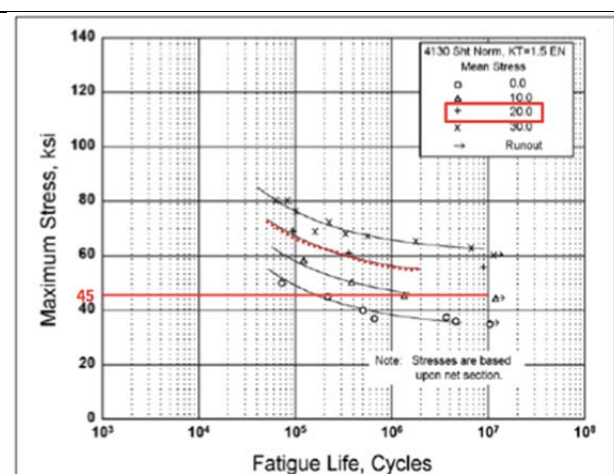


Figure 40: Stress life curves for $kt=1.5$ left side,

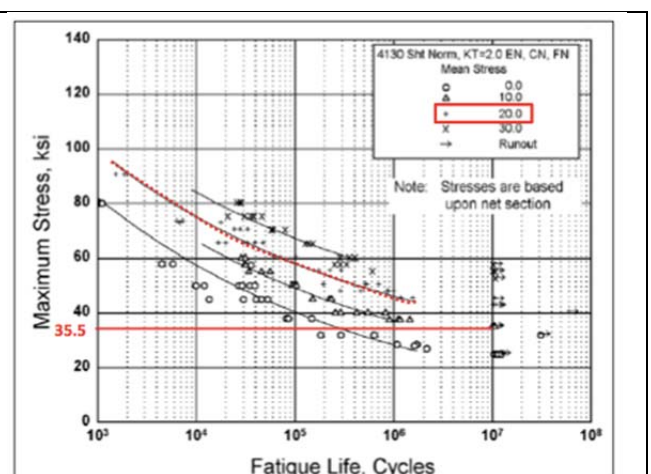


Figure 41: and $kt=2$ right side

Due to aging of the P-3 airplanes in civil operation, a careful inspection at the critical areas in the engine mount is absolutely mandatory.

We recommend the inspection of 5 locations in the area of the *Motorlasche* (engine connections) and *Anschlussbolzen* (upper and lower bolt connection to fuselage frame) every 100 FH or once a year.

4.11 References

- [1] «F/A-18 A/B Vertical Tail Stub Fatigue investigation», ASI Symposium 2011, Simon Barter
- [2] The Lead Crack Fatigue Lifting Framework, 2010, L. Molent, S. A. Barter, R. J. H. Wanhill
- [3] Structural Integrity of a Wing Upper Skin with Exfoliation Corrosion, M. Bos (ed.), ICAF 2009, Bridging the Gap between Theory and Operational Practice, 245–258, A. Uebersax, C. Huber, G. Renaud, M. Liao
- [4] <http://www.cleansky.eu/>
- [5] ED-WP_A.4.1-RA-RPT-0070_Demonstrator_A4_Technical_Requirements_and_Guidelines_A03
- [6] FEM-Test Results Correlation Study and Engineering Tool Chain Development for Clean Sky Eco Design Demonstrator A4, Master Thesis U. Stebler/ETHZ